

## NONLINEAR DIFFUSION FILTERING INFLUENCED BY MEAN CURVATURE\*

MICHAL KOLLÁR, KAROL MIKULA, RÓBERT ČUNDERLÍK†

**Abstract.** The paper introduces a new nonlinear diffusion filtering method on closed surfaces such as a sphere, ellipsoid or the Earth’s surface. Our new model extends the regularized surface Perona-Malik model by including a local extrema detector based on a mean curvature of processed data. The model is thus represented by a nonlinear diffusion equation which filters noise while preserves main edges, local extrema and details important for a correct interpretation of data. We define a surface finite-volume method to approximate numerically the nonlinear parabolic partial differential equation on a closed surface. The closed surface is approximated by a polyhedral surface created by planar triangles representing subdivision of an initial icosahedron grid and we use a piece-wise linear approximation of a solution in space and the backward Euler time discretization. Numerical experiments present nonlinear diffusion filtering of artificial data and real measurements, namely the GOCE satellite observations. They aim to point out a main advantage of the new nonlinear model which, on the contrary of Perona-Malik model, preserves local extremal values of filtered data.

**Key words.** data filtering, nonlinear diffusion equations, surface finite volume method, GOCE measurements

**AMS subject classifications.** 35R01, 65M08

**1. Introduction.** An important part of processing various kinds of measurements that contain noise and other inaccuracies is data filtering. There are many efficient filters that can reduce noise from observed data. Usually, linear filtering methods like the Gaussian, Wiener or Kalman filters are used to process data, however, these kinds of filters are based on a uniform smoothing effect. It means they successfully remove noise but at the same time smooth main structures. This can cause serious inaccuracies in filter results. Non-uniform smoothing of filtered data can be reached by nonlinear diffusion filters that can be locally adapted to data features, such as gradients or curvature of the noisy data. In this paper we focus on filtering methods mostly used in image processing that are based on the partial differential equations approach [1]. This approach is based on a simple observation that the Gauss function is fundamental solution of a linear heat (diffusion) equation. This provides a possibility to replace the uniform Gaussian filtering, which is based on a convolution of data with the Gauss function, by solving the linear diffusion equation with an initial condition given by the processed data. Nonlinear diffusion filters are based on an extension of the linear diffusion equation. At present, there are basically two kinds of nonlinear diffusion approaches. The first one is the regularized Perona-Malik model [7], where the diffusion coefficient depends on an edge detector [2]. The second approach known as a mean curvature flow model is based on a geometrical diffusion of level-sets of data.

In this paper we present an extension of nonlinear regularized surface Perona-Malik model considered on a closed surface and introduced in [3]. Our experiences

---

\*The work has been supported by the project APVV-0072-11 and the grants VEGA 1/0714/15 and VEGA 1/0608/15.

† Faculty of Civil Engineering, Slovak University of Technology in Bratislava, Radlinského 11, 813 68 Bratislava (kollarm@math.sk, mikula@math.sk, cunderli@svf.stuba.sk).

have shown that the Perona-Malik model successfully reduces noise while preserves edges but it smooths local extrema of filtered data. This drawback can be overcome by our modification, in which a diffusivity coefficient depends on the edge detector as well as on the mean curvature of filtered data. Such an approach prevents from smoothing of local extrema of filtered data.

The first part of the paper describes a modification of the linear diffusion on a closed surface to its nonlinear forms, namely the regularized surface Perona-Malik model and its extension by the local extrema detector. Then we derive a semi-implicit numerical scheme for the proposed nonlinear diffusion equation using the surface finite volume method. Finally, numerical experiments demonstrate advantages of such an approach comparing results with ones obtained by the linear diffusion and the Perona-Malik model.

**2. Diffusion filtering on a closed surface.** The linear diffusion of a scalar function  $u$  on a closed surface  $\Omega$  can be expressed by a parabolic partial differential equation in the form

$$(2.1) \quad \partial_t u = \Delta_s u,$$

where  $\Delta_s$  represents the generalized Laplace operator on a surface known as the Laplace-Beltrami operator. Eq. (2.1) corresponds to the heat equation on a closed surface. Its fundamental solution is given by the Gauss function. Consequently, a solution of the linear diffusion applied on some scalar function will be uniformly smoothed, similarly as the Gaussian filtering. On the contrary, nonlinear filtering allows nonuniform smoothing. This can be performed by a modification of the linear model by the nonlinear scalar diffusivity function  $g$  leading to the nonlinear diffusion equation [7]

$$(2.2) \quad \partial_t u = \nabla_s \cdot (g \nabla_s u).$$

In case of the regularized surface Perona-Malik model [3] the function  $g$  as a diffusivity coefficient depends on surface gradients

$$(2.3) \quad \partial_t u = \nabla_s \cdot (g(|\nabla_s u^\sigma|) \nabla_s u),$$

where  $g$  represents an edge detector in the form

$$(2.4) \quad g(|\nabla_s u^\sigma|) = \frac{1}{1 + K|\nabla_s u^\sigma|^2}, \quad K \geq 0,$$

where  $\nabla_s u^\sigma$  is a surface gradient of  $u$  smoothed by the linear surface diffusion in a short time interval  $\sigma$  and constant  $K$  represents sensitivity parameter. This parameter determines how sensitive will be edge detector to high values of a smoothed surface gradient of the function  $u$ .

As mentioned in the introduction, this model preserves edges, however, it can smooth local extrema of filtered data. It is due to the fact that the surface gradient in an area of local extrema is not high enough.

In this paper, we present the nonlinear diffusion filtering method where the function  $g$  depends on the surface gradient of a solution of the linear diffusion equation obtained for the short time step  $\sigma^1$  as well as on the mean curvature of a solution of the linear diffusion equation obtained for the short time step  $\sigma^2$ . Then the new nonlinear diffusion model has the form

$$(2.5) \quad \partial_t u = \nabla_s \cdot (g(|\nabla_s u^{\sigma^1}|, |\Delta_s u^{\sigma^2}|) \nabla_s u),$$

and the function  $g$  now depends on two parameters and can be written in the form

$$(2.6) \quad g(|\nabla_s u^{\sigma^1}|, |\Delta_s u^{\sigma^2}|) = \frac{1}{1 + K_1 |\nabla_s u^{\sigma^1}|^2 + K_2 |\Delta_s u^{\sigma^2}|^2}, \quad K_1, K_2 \geq 0.$$

This extension results in the diffusion process slowed down in areas where the function  $u$  has generally high mean curvature. These areas particularly represent local extrema of the function  $u$ . So the function in this form can be called edge and local extrema detector. The parameter  $K_1$  has the same meaning as in the edge detector in the Perona-Malik model and the parameter  $K_2$  affects sensitivity to high values of the mean curvature of the function  $u$ . Since our computational domain  $\Omega$  is the closed surface we do not need any boundary conditions for Eq. (2.5).

**3. The surface finite volume method for the new nonlinear diffusion model.** The differential equation (2.5) is numerically solved by a surface finite volume method [3][6]. In this approach, the closed computational domain  $\Omega$  is approximated by an appropriate triangulation defined by  $N$  representative nodes,  $X_i, X_i \subset \Omega, i = 1, \dots, N$ . These nodes represent vertices of the triangular grid defined by planar triangles  $T_{iq}, q = 1, \dots, Q_i, i = 1, \dots, N$ , where  $Q_i$  is the number of triangles with the vertex  $X_i$ . Other two vertices of the triangle  $T_{iq}$  will be denoted by  $X_i^{q1}$  and  $X_i^{q2}$ . A value of the scalar function  $u$  in the node  $X_i$  is denoted by  $u_i$ . On the given triangulation we construct a finite volume grid. At each node  $X_i$  we create a co-volume  $V_i$  bounded by straight lines that connect midpoints between  $X_i$  and its neighbours  $X_i^{q1}, X_i^{q2}$  with centers of mass of all triangles joined in the node  $X_i$  (see Fig. 3.1).

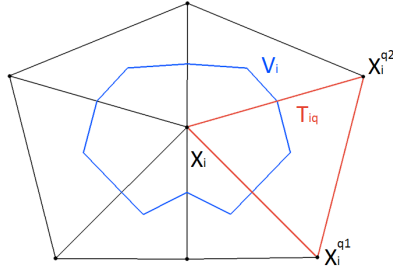


Fig. 3.1: Finite volume  $V_i$

The numerical scheme is derived in the sequel. By integrating (2.5) over the finite volume  $V_i$  and by applying Green's theorem we obtain

$$(3.1) \quad \int_{V_i} \partial_t u \, dx = \int_{\partial V_i} g(|\nabla_s u^{\sigma^1}|, |\Delta_s u^{\sigma^2}|) \nabla_s u \cdot \vec{\eta}_i \, ds,$$

where  $\nabla_s u$  represents the surface gradient of the function  $u$  and  $\vec{\eta}_i$  is a unit outward normal to the boundary  $\partial V_i$ . The integral over the co-volume boundary  $\partial V_i$  can be, taking into account geometry of this boundary, expressed in the form of a sum of integrals over each part of the boundary

$$(3.2) \quad \int_{V_i} \partial_t u \, dx = \sum_{q=1}^{Q_i} \int_{\partial V_{iq}} g(|\nabla_s u^{\sigma^1}|, |\Delta_s u^{\sigma^2}|) \nabla_s u \cdot \vec{\eta}_{iq} \, ds,$$

where  $\partial V_{iq}$  are parts of the co-volume boundary, subset of  $T_{iq}$ , with normal vectors  $\vec{\eta}_{iq}$  (see Figure 3.2).

Equation (2.5) is solved in a time interval  $[0, T]$ . This interval is divided into  $M$  time steps  $t_j$ ,  $j = 1, \dots, M$  and the time derivative  $\partial_t u$  is approximated by the backward Euler difference  $\partial_t u = \frac{u^j - u^{j-1}}{\tau}$ , where  $\tau = t_j - t_{j-1}$  denotes the time step and the value of  $u^j$  represents a solution in the  $j^{th}$  time step. Hence, the left hand side of the Eq. (3.2) can be approximated by  $m(V_i) \frac{u_i^j - u_i^{j-1}}{\tau}$ , where  $m(V_i)$  represents an area of the co-volume  $V_i$ . Then approximation of (2.5) can be rewritten in the form

$$(3.3) \quad m(V_i) \frac{u_i^j - u_i^{j-1}}{\tau} = \sum_{q=1}^{Q_i} \int_{\partial V_{iq}} g(|\nabla_s u^{\sigma^1}|, |\Delta_s u^{\sigma^2}|) \nabla_s u^j \cdot \vec{\eta}_{iq} ds.$$

If we consider a linear representation of  $u^j$  on each triangle, the surface gradient  $\nabla_s u^j$  is a constant vector over each triangle  $T_{iq}$  and by using the mean value theorem and Green's theorem we get

$$(3.4) \quad \nabla_s u^j \approx \frac{1}{m(T_{iq})} \int_{T_{iq}} \nabla_s u^j ds = \frac{1}{m(T_{iq})} \int_{\partial T_{iq}} u^j \cdot \vec{n}_{iq} ds,$$

where  $m(T_{iq})$  is an area of the triangle  $T_{iq}$  and  $\vec{n}_{iq}$  is the unit outward normal to the boundary of the triangle  $T_{iq}$ . If we consider the linear approximation of the solution, the integral over the triangle boundary can be expressed as a sum of average values from each triangle side. If we denote the constant value of the surface gradient on the triangle  $T_{iq}$  by  $P_{T_{iq}}^j$ , we obtain

$$(3.5) \quad P_{T_{iq}}^j = \frac{1}{m(T_{iq})} \left( \frac{u_i^j + u_{q1}^j}{2} d_{iq1} \vec{n}_{iq1} + \frac{u_i^j + u_{q2}^j}{2} d_{iq2} \vec{n}_{iq2} + \frac{u_{q1}^j + u_{q2}^j}{2} d_{q1q2} \vec{n}_{q1q2} \right)$$

Nodal values of the solution, sizes of the triangular sides and their normal vectors are denoted according to Figure 3.2.

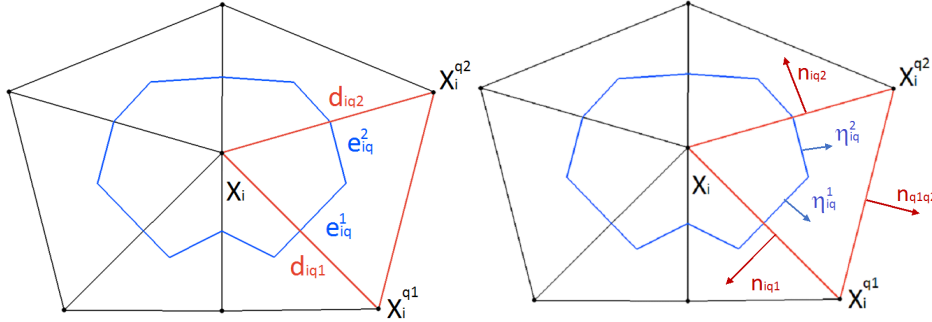


Fig. 3.2: Plot of the sides of the triangle  $T_{iq}$ ,  $d_{iq1}$ ,  $d_{iq2}$ ,  $d_{q1q2}$ , and portions of the co-volume boundary  $e_{iq}^1$ ,  $e_{iq}^2$  inside triangle  $T_{iq}$ . Outward unit normal vectors to the triangle  $T_{iq}$ ,  $\vec{n}_{iq1}$ ,  $\vec{n}_{iq2}$ ,  $\vec{n}_{q1q2}$ , and to the co-volume boundary,  $\eta_{iq}^1$ ,  $\eta_{iq}^2$ .

The second argument of the detector function in Eq. (2.6) represents the mean curvature of  $u$  smoothed by the linear diffusion in short time interval  $\sigma^2$ . In the case  $g = 1$  we get a linear diffusion process. Using Eq. (3.3) and Eq. (3.5) we can define an approximation of the mean curvature on the co-volume in the form

$$(3.6) \quad \Delta_s u^j \approx \frac{1}{m(V_i)} \sum_{q=1}^{Q_i} \int_{\partial V_{iq}} P_{T_{iq}}^j \cdot \vec{\eta}_{iq} ds.$$

Since  $P_{T_{iq}}^j$  is a constant vector and  $\int_{\partial V_{iq}} \vec{\eta}_{iq} = m(e_{iq}^1) \vec{\eta}_{iq}^1 + m(e_{iq}^2) \vec{\eta}_{iq}^2$ , where  $m(e_{iq}^1)$  and  $m(e_{iq}^2)$  are lengths of the parts of the co-volume boundaries in the triangle  $T_{iq}$ , we can denote a value of the mean curvature on the co-volume by  $C_i^j$  and we obtain

$$(3.7) \quad C_i^j = \frac{1}{m(V_i)} \sum_{q=1}^{Q_i} \left[ m(e_{iq}^1) \vec{\eta}_{iq}^1 \cdot P_{T_{iq}}^j + m(e_{iq}^2) \vec{\eta}_{iq}^2 \cdot P_{T_{iq}}^j \right].$$

An average value of mean curvature on the triangle  $T_{iq}$  can be denoted as

$$(3.8) \quad C_{T_{iq}}^j = \frac{1}{3} (C_i^j + C_{q_1}^j + C_{q_2}^j),$$

where  $C_i^j$ ,  $C_{q_1}^j$  and  $C_{q_2}^j$  represents nodal values of the mean curvature evaluated in all three vertices of the triangle.

After some simple manipulations in Eq. (3.3), using similar approach as in the previous equations, we obtain a semi-implicit numerical scheme for the new nonlinear filtration method on the closed surface in the form

$$(3.9) \quad u_i^j - \frac{\tau}{m(V_i)} \sum_{q=1}^{Q_i} \left[ m(e_{iq}^1) \vec{\eta}_{iq}^1 \cdot P_{T_{iq}}^j g(|P_{T_{iq}}^{\sigma^1, j-1}|, |C_{T_{iq}}^{\sigma^2, j-1}|) \right. \\ \left. m(e_{iq}^2) \vec{\eta}_{iq}^2 \cdot P_{T_{iq}}^j g(|P_{T_{iq}}^{\sigma^1, j-1}|, |C_{T_{iq}}^{\sigma^2, j-1}|) \right] = u_i^{j-1}$$

where  $P_{T_{iq}}^{\sigma^1, j-1}$  is an approximation of the smoothed gradient of the solution from the previous time step  $j-1$ , and analogously,  $C_{T_{iq}}^{\sigma^2, j-1}$  is an approximation of the smoothed average mean curvature of the solution on the triangle at the time step  $j-1$ .

Eq. (3.9) represents an approximation of the nonlinear diffusion equation (2.5) in one finite volume  $V_i$ , so the approximation over all finite volumes  $V_i$ ,  $i = 1, \dots, N$  is defined by a linear system of equations  $Au^j = u^{j-1}$ . The matrix  $A$  is the system matrix with coefficients dependent on the time step and triangulation. Matrix positions of non-zero coefficients depend on the number of neighbours of the node  $X_i$ . The linear system is then solved by the SOR algorithm. To obtain the matrix  $A$  diagonally dominant, we choose the time step  $\tau$  proportional to the average area of co-volumes

$$(3.10) \quad \tau = \frac{1}{N} \sum_{i=1}^N m(V_i).$$

**4. Numerical experiments and results.** We present two numerical experiments. The first one represents a testing experiment. Its principal goal is to show how a chosen artificial data  $u$  is changed while using different filtering methods. This experiment highlights main and significant differences between behavior of the filters. The second experiment presents filtering of measurements of the GOCE satellite mission, namely  $T_{zz}$  as the second derivative of disturbing potential in the radial direction. In both numerical experiments, we approximate a spherical computational domain with an appropriate well-oriented triangulation. It is represented by a subdivision of an initial icosahedron grid known also as a geodetic grid. The process of subdivision can be seen in Figure 4.1. The main advantage of this type of grid is its

uniformity. Almost all co-volumes defined on this grid are hexagons only twelve of co-volumes will be pentagons and area of each co-volume is almost the same.

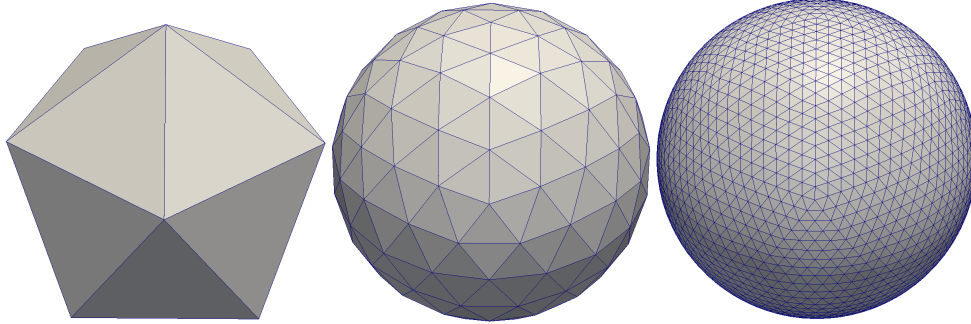


Fig. 4.1: Icosahedron subdivision: original icosahedron grid, grid after 2 subdivision and after 4 subdivision

**4.1. Testing experiment.** In the testing experiment we study a different behavior of three different filtering methods, namely the linear diffusion model, the nonlinear Perona-Malik model and our new nonlinear model. We use the icosahedron grid  $\Omega$  formed by 163842 nodes and 327680 triangles which represents eight subdivision of the original icosahedron grid. To create artificial data  $u$  we use a function with compact support in the form

$$(4.1) \quad u(\mathbf{x}) = v \cdot e^{\frac{-\sigma}{(r^2 - |\mathbf{x} - \mathbf{s}|^2) + \frac{\sigma}{r^2}}}$$

if  $|\mathbf{x} - \mathbf{s}| < r$  and  $u(\mathbf{x}) = 0$  if  $|\mathbf{x} - \mathbf{s}| \geq r$ , where  $\mathbf{s}(s_1, s_2, s_3) \in \Omega$  and  $\mathbf{x}(x_1, x_2, x_3) \in \Omega$ . We set  $v = 0.4$ ;  $\sigma = 5r^2$ ;  $r = 0.2$  and  $\mathbf{s}(s_1, s_2, s_3) = (0, -0.52573, 0.85065)$ . Figure 4.2 depicts an intersection through chosen nodes from original data and results obtained after 50 and 100 time steps of each kind of diffusion filter. In case of the nonlinear Perona-Malik model we use the sensitivity coefficient  $K = 10$  for the edge detector. In our new nonlinear method, we use the sensitivity coefficients  $K_1, K_2$  for edge and local extrema detector as  $K_1 = 10$ ,  $K_2 = 0.01$ . In the figures corresponding to the Perona-Malik and new model, initial values of the edge and local extrema detector before the first time step are visualized. The scale for detector values on the right side of the figures is reversed.

The intersections in Figure 4.2a) through results of the linear diffusion filter confirms a uniform smoothing effect. A nonuniform smoothing effect we obtained by using the nonlinear Perona-Malik model and our new nonlinear model. In Figure 4.2b) we can see that the Perona-Malik model preserves edges of artificial data. The red line in Figures represents values of edge detector on corresponding nodes. On edges, values of the detector are almost zero and for this reason the diffusion process is remarkably slowed. Values of the edge detector enlarge toward a top of the data and as we can see in results after 50 and 100 time step, local extrema of the data is pulled down. Figure 4.2c) represents an intersection through results of the new nonlinear model. Visualized values of the edge and local extrema detector are zero almost over whole testing artificial data. The local extrema detector detects high values of mean curvature along edges and in areas of data extrema. This will cause that the original data will barely change over time steps.

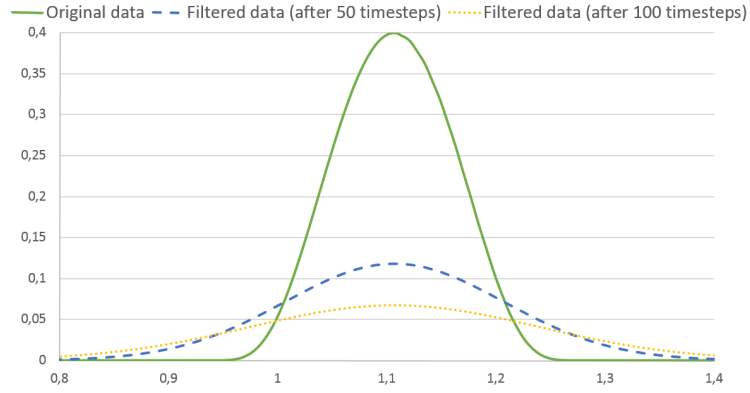
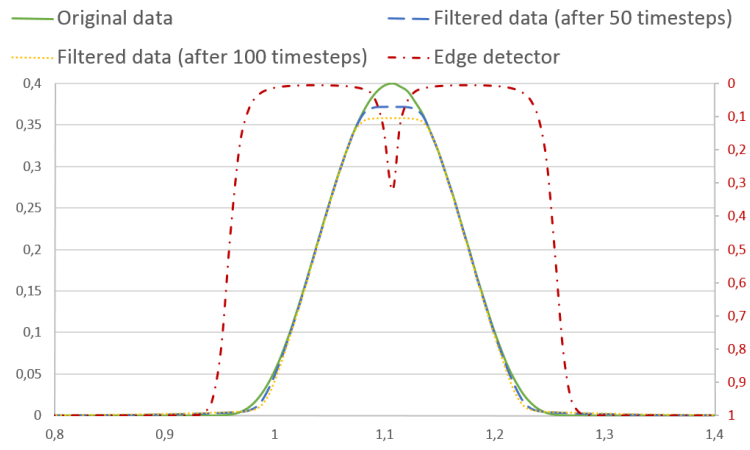
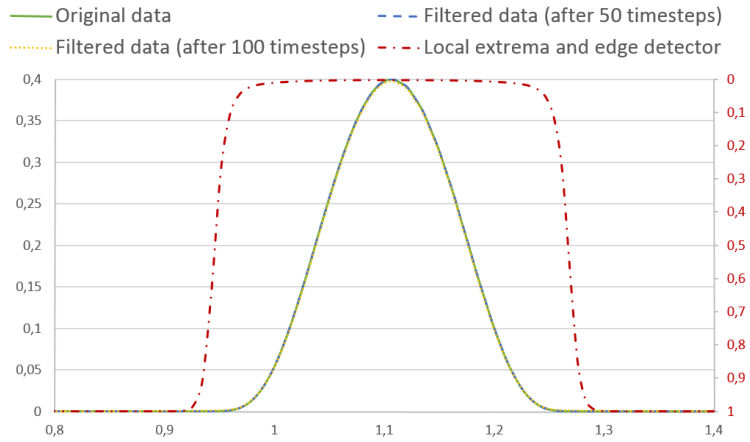

 (a) Linear diffusion of  $u$ 

 (b) Nonlinear Perona-Malik diffusion of  $u$ 

 (c) New nonlinear diffusion of  $u$ 

Fig. 4.2: Intersections through results of the testing experiment

**4.2. Filtering the GOCE measurements.** In this experiment, we focus on removal of noise from measurements of the GOCE satellite mission. An objective of this mission was to monitor the static part of the Earth's gravity field [5]. In this paper we process data observed during June-July 2013. Due to variations of the GOCE satellite orbits, observed data were reduced to the reference altitude 245km [4]. In this experiment, we use a finer grid, which represents the ninth subdivision of icosahedron. Grid contains 655 362 nodes and 1 310 720 triangles. These GOCE measurements mapped to the grid are subsequently filtered by our new nonlinear diffusing filtering method.

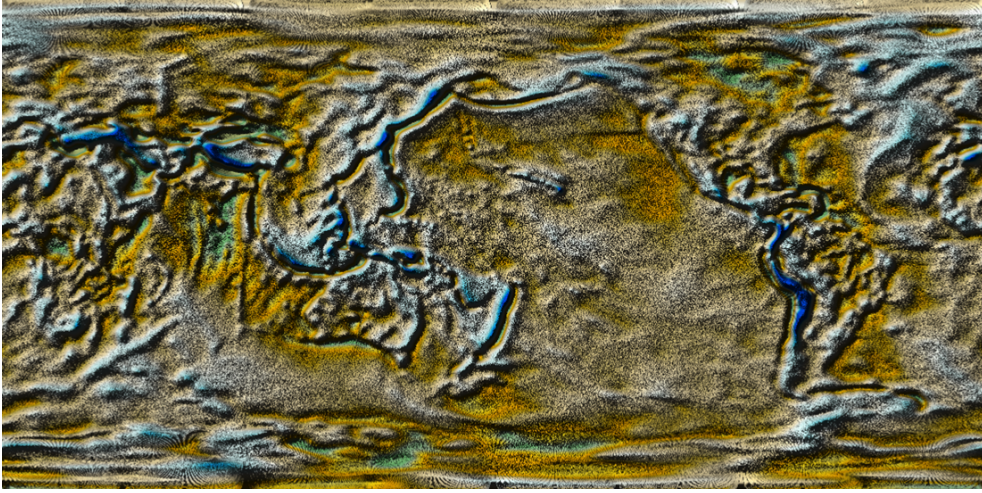


Fig. 4.3: Original GOCE measurement

At the beginning we need to set acceptable model parameters. For the edge and local extrema detector we need to set small time steps for pre-smoothing by the linear diffusion as well as sensitivity coefficients. The reason for appropriate selection of linear diffusion time step is that we need to smooth most of noise before we quantify surface gradients and mean curvatures. The differences between gradients and mean curvature in the data from the first quarter of equatorial intersection before and after linear diffusion are in Figure 4.4 and in Figure 4.5. We can see that before pre-filtering by the linear diffusion, high values of gradients and mean curvature are almost everywhere. After the linear diffusion the noise is removed and values of the gradient and mean curvature reflect structures of the Earth's gravity field. Experimentally (considering different input parameter) we choose suitable time steps for the linear diffusion as  $\sigma^1 = \sigma^2 = \frac{1}{4}\tau$ , time step for nonlinear diffusion as  $\tau$  and the sensitivity coefficients as  $K_1 = 0.2$ ,  $K_2 = 0.2 \cdot 10^{-4}$ . Figure 4.6 presents different segments of equatorial intersections through results obtained after different time steps.



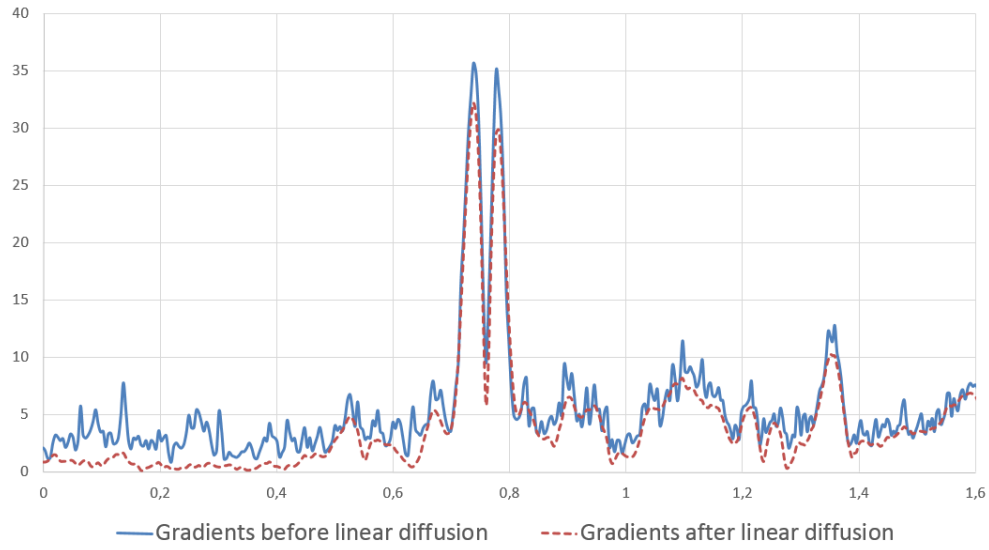


Fig. 4.4: Gradients of the data before and after linear diffusion

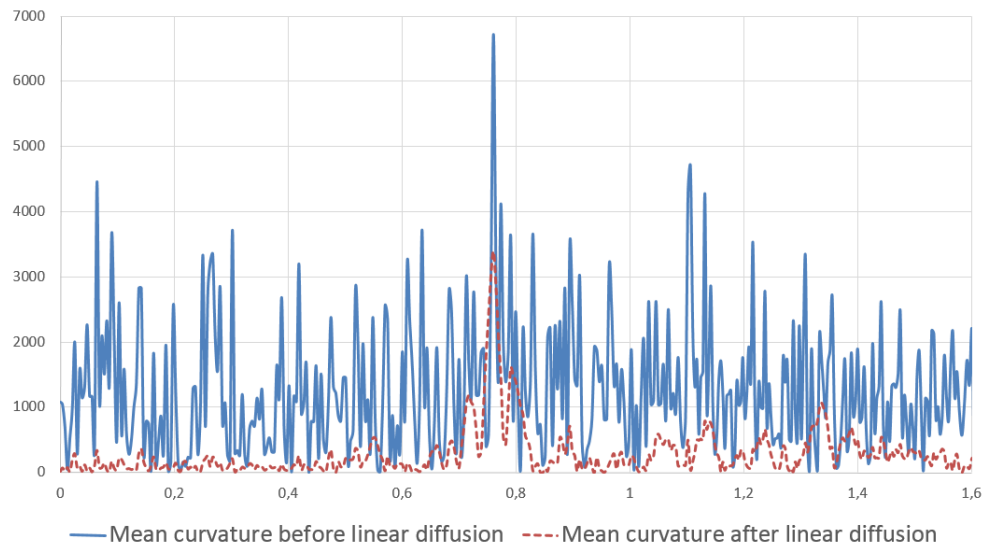
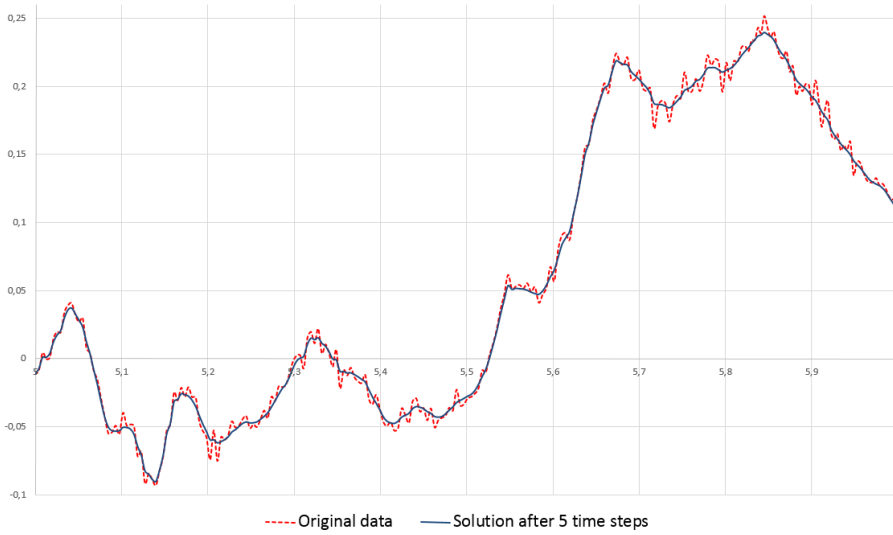


Fig. 4.5: Mean curvature of the data before and after linear diffusion



(a) Part of equatorial intersection from result after 5 time steps



(b) Part of equatorial intersection from result after 5 time steps

Fig. 4.6: Results of GOCE measurement filtering

To demonstrate advantages of our new nonlinear model, Figure 4.7 shows a detail from original data and visualization of differences between solution obtained by the Perona-Malik model with  $K = 0.2$  and the new nonlinear diffusion model with  $K_1 = 0.2, K_2 = 0.2 \cdot 10^{-4}$  from the same detail area after 5 time steps of filtering. From Figure 4.7 is obvious that maximal differences between solutions are in areas of local extrema of original data. Both models successfully remove noise, but the Perona-Malik model also smooths local extrema representing important structures in the filtered data. On the contrary, the new nonlinear diffusion model, whose edge detector is extended by the local extrema detector, obviously preserves signal better in areas of local extrema. It confirms that high values of the mean curvature in areas of

local extrema yield small values of the diffusivity coefficient while avoiding undesired smoothing.

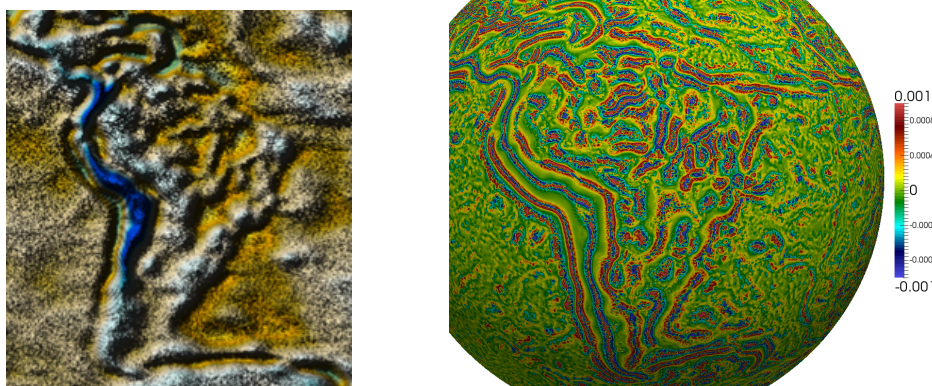


Fig. 4.7: Detail from original data and visualization of differences between solution obtained by Perona-Malik and new model.

**5. Conclusion.** The presented nonlinear filter is based on a numerical solution of the nonlinear diffusion equation, where the diffusivity coefficient represent a combination of the edge detector and local extrema detector. The semi-implicit numerical scheme, derived using the proposed surface finite volume method, is efficient to numerically approximate surface gradients as well as the Laplace-Beltrami operator. Numerical experiments show that both the Perona-Malik and extended model have adaptive and the non-uniform smoothing effect. The obvious advantage of the presented approach can be seen in its comparison with the Perona-Malik. The Perona-Malik model smoothes local extrema of filtered data because the diffusivity coefficient is purely based on the edge detector. Its extension by the local extrema detector which captures high values of the mean curvature of filtered data allows to slow down diffusion effect also on those areas. Thus the proposed extension is highly efficient and can be used for filtering various kinds of data.

#### REFERENCES

- [1] ALVAREZ L, GUICHARD F, LIONS PL, MOREL JM, *Axioms and fundamental equations of image processing.*, Arch Ration Mech. 1991, p. 199-257
- [2] CATTÉ F, LIONS PL, MOREL JM, COLL T, *Image selective smoothing and edge detection by nonlinear diffusion.*, SIAM J Numer Anal 29. 1992, p. 182193
- [3] ČUNDERLÍK R, MIKULA K, TUNEGA M, *Nonlinear diffusion filtering of data on the Earth's surface*, Journal of Geodesy. 2012, p. 143-160, ISSN 0949-7714
- [4] ČUNDERLÍK R, *Precise Modelling of the Static Gravity Field from GOCE Second Radial Derivatives of the Disturbing Potential Using the Method of Fundamental Solutions*, In: International Association of Geodesy Symposia, DOI 10.1007/1345\_2015\_211, Springer (in press)
- [5] ESA, *Gravity field and steady-state ocean circulation mission. Report for mission selection of the four candidate earth explorer missions*, ESA SP-1233(1), ESA Publications Division, 1999, ESTEC, Noordwijk, The Netherlands.
- [6] EYMARD R, GALLOUET T, HERBIN R, *Finite Volume Methods*, Handbook of Numerical Analysis P.G. Ciarlet, 1997, J.L. Lions eds, vol 7, pp 713-1020
- [7] PERONA P, MALIK J, *Scale space and edge detection using anisotropic diffusion.*, Proceedings of the IEEE society workshop on computer vision. 1987